Published as: *Development*. 2010 May ; 137(9): 1563–1571.

von Hippel-Lindau protein regulates transition from fetal to adult circulatory system in retina

Toshihide Kurihara[1,2,3,7,*], **Yoshiaki Kubota**[4,*], **Yoko Ozawa**[1,2,3], **Keiyo Takubo**[4], **Kousuke Noda**[3,8], **M. Celeste Simon**[6], **Randall S. Johnson**[7], **Makoto Suematsu**[5], **Kazuo Tsubota**[2], **Susumu Ishida**[3,8], **Nobuhito Goda**[9], **Toshio Suda**[4], and **Hideyuki Okano**[1]

[1]Department of Physiology, Keio University School of Medicine, 35 Shinanomachi, Shinjuku-ku, Tokyo 160-8582, Japan

[2]Department of Ophthalmology, Keio University School of Medicine, 35 Shinanomachi, Shinjuku-ku, Tokyo 160-8582, Japan

[3]Laboratory of Retinal Cell Biology, Keio University School of Medicine, 35 Shinanomachi, Shinjuku-ku, Tokyo 160-8582, Japan

[4]Department of Cell Differentiation, The Sakaguchi Laboratory, Keio University School of Medicine, 35 Shinanomachi, Shinjuku-ku, Tokyo 160-8582, Japan

[5]Department of Biochemistry and Integrative Medical Biology, Keio University School of Medicine, 35 Shinanomachi, Shinjuku-ku, Tokyo 160-8582, Japan

[6]Abramson Family Cancer Research Institute and Howard Hughes Medical Institute, University of Pennsylvania School of Medicine, 421 Curie Boulevard, Philadelphia, Pennsylvania 19104, USA

[7]Molecular Biology Section, Division of Biological Sciences, University of California San Diego, 9500 Gilman Drive, La Jolla, California 92093-0366, USA

[8]Department of Ophthalmology, Hokkaido University Graduate School of Medicine, Kita 8, Nishi 5 Kita-ku, Sapporo, Hokkaido, Japan

[9]Department of Life Science and Medical Bio-Science, School of Advanced Science and Engineering, Waseda University, 2-2 Wakamatsu-cho, Shinjuku-ku, Tokyo, 162-8480, Japan

SUMMARY

In the early neonatal stage, the fetal circulatory system undergoes dramatic transition to the adult circulatory system. Normally, embryonic connecting vessels such as ductus arteriosus and the foramen ovale close and regress. In the neonatal retina, hyaloid vessels maintaining blood flow in the embryonic retina regress, and retinal vessels take over to form adult-type circulatory system. This process is regulated by the programmed cell death switch mediated by macrophages via Wnt and Angiopoietin-2 pathways. In this study, we seek for the other mechanisms that regulate this process, and focus on the dramatic change in oxygen environment at the point of birth. The von Hippel–Lindau tumor suppressor protein (pVHL) is a substrate recognition component of an E3-ubiquitin ligase that rapidly destabilizes hypoxia-inducible factor-αs (HIF-αs) under normoxic conditions, but not hypoxic conditions. To examine the role of oxygen-sensing mechanisms in the retinal circulatory system transition, we generated retina-specific conditional knockout mice for

Corresponding authors: Hideyuki Okano, M.D., Ph.D., Professor and Chairman, Department of Physiology, Keio University School of Medicine, 35 Shinanomachi, Shinjuku-ku, Tokyo 160-8582, Japan, Phone: 81-3-5363-3747, Fax: 81-3-3357-5445, hidokano@sc.itc.keio.ac.jp. Toshio Suda, M.D., PhD., Professor and Chairman, Department of Cell Differentiation, The Sakaguchi Laboratory, Keio University School of Medicine, 35 Shinanomachi, Shinjuku-ku, Tokyo 160-8582, Japan, Phone: 81-3-5363-3475, FAX: 81-3-5363-3475, sudato@sc.itc.keio.ac.jp.
*These authors contributed equally to this work.

VHL *(VHL$^{\alpha\text{-}Cre\ KO}$* mice). These mice exhibit arrested transition from fetal to adult circulatory system: persistence of hyaloid vessels and poorly formed retinal vessels. These defects are suppressed by intraocular injection of Flt1-Fc protein (vascular endothelial growth factor (VEGF) Receptor-1 (Flt1)/Fc chimeric protein that can bind VEGF and inhibit its activity), or by inactivating the HIF-1 α gene. Our results suggest that not only macrophages but also tissue oxygen-sensing mechanisms regulate the transition from fetal to adult circulatory system in retina.

Keywords

Angiogenesis; Circulatory system; Hypoxia-inducible factor 1

INTRODUCTION

In the early neonatal stage, the fetal circulatory system undergoes rapid and dramatic transition to the adult circulatory system to adapt to detachment from the blood supply from maternal bodies. Normally, embryonic connecting vessels such as ductus arteriosus, ductus venosus and the foramen ovale close and regress (Merkle and Gilkeson, 2005). In the neonatal retina, it is generally known that hyaloid vessels maintaining blood flow in the embryonic retina regress, and retinal vessels assume the role of supplying blood for the retina (Lang, 1997; Lobov et al., 2005). This process is regulated by the programmed cell death switch mediated by macrophages via Wnt and Angiopoietin-2 pathways (Lang and Bishop, 1993; Lobov et al., 2005; Rao et al., 2007).

Oxygen concentration is vital to nearly all forms of life on earth via its role in energy homeostatic regulation (Yun et al., 2002). Mammalian embryos develop in a low oxygen environment inside the maternal body – approximately 3% oxygen (Rodesch et al., 1992). However, pups are abruptly exposed to atmosphere (approximately 21% oxygen) after birth. This dramatic change in oxygen environment at the point of birth indicates some critical roles of oxygen concentration in triggering the transition from fetal to adult circulatory system.

The von Hippel–Lindau tumor suppressor protein (pVHL) is a substrate recognition component of an E3-ubiquitin ligase that rapidly destabilizes hypoxia-inducible factor-αs (HIF-αs) under normoxic conditions, but not hypoxic conditions (Maxwell et al., 1999). Genetic inactivation of the VHL gene results in stabilization and increased activity of HIF-αs, which includes HIF-1α, HIF-2α, and HIF-3α. It has been reported that VHL-null embryos are lethal at El 1.5–12.5 due to abnormal placental vascularization (Gnarra et al., 1997). Endothelial-specific deletion of VHL gene utilizing Tie2-Cre mice also results in intrauterine death with hemorrhage at E12.5, and loss of HIF-1 α did not rescue the lethality (Tang et al., 2006). Although vascular endothelial growth factor (VEGF) is widely known as a HIF-1 α target gene (Forsythe et al., 1996), HIF-2α is thought to be the main regulator of VEGF in tissues that express both HIF-1 α and HIF-2α (Hu et al., 2003; Tang et al., 2006). These previous studies showed that VHL is required for endothelial cells in a cell autonomous manner. However, surprisingly, it is still largely unknown how VHL contributes to vascular development, particularly how and when the well-known relationship between VHL and oxygen concentration operates vascular development. In human, VHL disease is an autosomal dominant syndrome that causes the development of various benign and malignant disorders (Nicholson et al., 1976). The major disorders include retinal, brain and spinal cord angioma, pheochromocytoma, renal cell carcinoma, and pancreatic cystadenoma. In the majority of VHL patients, retinal angioma is the first sign of the disease to appear. However, the molecular mechanism of retinal angioma development in VHL disease still remains unknown.

In this study, utilizing retina-specific conditional knockout technology, we explored the precise *in vivo* function of VHL in retinal vascular development, and showed that not only macrophages but also tissue oxygen-sensing mechanisms regulate the transition from fetal to adult circulatory system in retina.

MATERIALS AND METHODS

Mice

All animal experiments were conducted in accordance with the Association for Research in Vision and Ophthalmology (ARVO) Statement for the Use of Animals in Ophthalmic and Vision Research. In the expression analysis shown in Fig. 1, we used C57BL/6 mice (Clea Japan). Transgenic mice expressing Cre recombinase under control of the *Pax6* retina-specific regulatory element, α-promoter (*α-Cre*) (Marquardt et al., 2001), were mated with $VHL^{floxed/floxed}$ mice (Haase et al., 2001) (kind gift from Volker H. Haase, University of Pennsylvania), $HIF\text{-}1\alpha^{floxed/floxed}$ mice (Ryan et al., 2000), or $HIF\text{-}2\alpha^{floxed/floxed}$ mice (Gruber et al., 2007). As control littermates for $VHL^{\alpha\text{-}Cre\ KO}$ mice, $HIF\text{-}1\alpha^{\alpha\text{-}Cre\ KO}$ mice, $HIF\text{-}1\alpha^{\alpha\text{-}Cre\ KO}$;$VHL^{\alpha\text{-}Cre\ KO}$ mice, or $HIF\text{-}2\alpha^{\alpha\text{-}Cre\ KO}$;$VHL^{\alpha\text{-}Cre\ KO}$ mice, we used $VHL^{floxed/floxed}$ mice. $HIF\text{-}1\alpha^{floxed/floxed}$ mice. $HIF\text{-}1\alpha^{floxed/floxed}$ $VHL^{floxed/floxed}$ mice or $HIF\text{-}2\alpha^{floxed/floxed}$; $VHL^{floxed/floxed}$ mice without α-Cre transgene, respectively. In a preliminary study, we found no detectable difference in retinal vascular structures between a-Cre+ and a-Cre- mice confirming the validity of these control littermates. To monitor the Cre expression in *α-Cre* mice or $VHL^{\alpha\text{-}Cre\ KO}$ mice, we mated these mice with CAG-CAT-EGFP transgenic mice (Kawamoto et al., 2000), respectively. All mice used in this study were maintained on a C57BL/6J background.

Preparation of whole-mount samples and cryosections of retinas

Enucleated eyes were fixed for 20 min in 4% paraformaldehyde (PFA) in PBS and then dissected as previously described (Fruttiger et al., 1996; Gerhardt et al., 2003; Kubota et al., 2008). The obtained tissues were post-fixed overnight in 4% PFA in PBS and stored in methanol at −20 °C. Cryosections of retinas (10 μm) were prepared as previously described (Kurihara et al., 2006) after eye balls were immersed overnight in 4% PFA.

Immunostaining and in situ hybridization

Immunohistochemistry (IHC) for whole-mount retinas and other tissues was performed as described previously (Fruttiger et al., 1996; Gerhardt et al., 2003; Kubota et al., 2008; Kurihara et al., 2006). The primary antibodies used were monoclonal anti-PECAM-1 (2H8, Chemicon), α-smooth muscle actin (1A4; FITC-conjugated; Sigma-Aldrich), desmin (DAKO), F4/80 (A3-1; Serotec, Oxford, UK), and GFAP (G-A-5; Cy3-conjugated; Sigma-Aldrich or Dako), polyclonal type IV collagen (Cosmo Bio), HIF-1α (originally established by immunizing purified fusion proteins encompassing amino acids 416 to 785 of mouse HIF-1α into guinea pigs), HIF-2α (Santa Cruz Biotechnology), glutamine synthetase (Molecular Probes), opsin (Cosmo Bio) and pVHL (Santa Cruz Biotechnology). The secondary antibodies used were Alexa Fluor 488 conjugated IgGs (Molecular Probes) or Cy3/Cy5 conjugated IgGs (Jackson ImmunoResearch). Nuclei were stained with 10 μg/ml Hoechst bisbenzimide 33258 (Sigma-Aldrich) or DAPI (Molecular Probes). For whole-mount in situ hybridization (ISH), retinas were briefly digested with proteinase K and hybridized with digoxigenin (DIG)-labeled antisense RNA probes. When ISH was combined with IHC, IHC was performed after all the ISH procedures were completed. For the BrdU incorporation assay, 100 μg per body weight (g) of BrdU (BD Pharmingen) dissolved in sterile PBS was injected intraperitoneally 2 hours before sacrifice. Isolated retinas were stained using a BrdU immunohistochemistry system (Calbiochem) according to the manufacturer's instructions. When BrdU assays were combined with IHC, the application of

first antibodies was done simultaneously. FITC-conjugated Dextran (Sigma-Aldrich) was injected into the left cardiac ventricle and allowed to circulate for 2 min. After staining, samples were mounted using a Prolong Antifade Kit (Molecular Probes).

Assessment of tissue hypoxia

Detection of hypoxic cells in cryosections was performed using a Hypoxyprobe-1 Plus Kit (Chemicon). In brief, 60 mg/kg of pimonidazole was injected intraperitoneally 30 min before sacrifice, and samples were stained with Hypoxyprobe Mabl-FITC.

RT-PCR analysis

Total RNA was prepared from retinal tissues and reverse-transcribed using Superscript II (Invitrogen). A quantitative PCR assay for *vegfa* was performed on an ABI7500 Fast Real-Time PCR System using TaqMan Fast Universal PCR master mixture (Applied Biosystems) and TaqMan® Gene Expression Assay Mix of *vegfa* (Mm00437304_ml), *csflr* (Mm00432689_ml), and *angiopoietin-2* (Mm00545822_ml). Mouse β-actin (Mm00607939_s 1) assay mix served as endogenous control. Data were analyzed with 7500 Fast System SDS Software 1.3.1. All experiments were done with four replicates.

Intra-vitreous injections

Injections into the vitreous body were performed using 33-gauge needles as described previously (Gerhardt et al., 2003; Kubota et al., 2008). Sterile PBS (0.5 μ1) with or without 1 mg/ml of Fltl-Fc chimera proteins (R&D Systems) was injected at P4.

Confocal microscopy and quantification

Fluorescence images were obtained using a confocal laser scanning microscope (FV1000; Olympus) at room temperature. Quantification of the cells or substances of interest was usually done in eight random 200 μm × 200 μm fields just behind the sprouting edges of each retina. To construct three-dimensional projections, multiple slices horizontally imaged from the same field of view were integrated by FV10-ASW Viewer (Olympus).

Retinal explant culture

Retinal explant culture was performed using P6 mouse neural retinas based on the protocol we previously described (Ozawa et al., 2007; Ozawa et al., 2004). Briefly, eyes were enucleated and neural retinas were isolated and placed on a Millicell chamber filter (Millipore: pore size: 0.4 Am) with the ganglion cell layer facing up. The chamber was then placed in a 6-well culture plate, containing 50% MEM (GIBCO), 25% HBSS (GIBCO), 25% horse serum (Thermo Trace), 200 mM L-glutamine, and 6.75 mg/ml D-glucose. Explants were incubated at 34°C in 5% CO_2. 24 hours after exposure of each concentration of oxygen, the explants were subjected to immunestaining or RT-PCR analysis. The oxygen concentration in the incubator was controlled with nitrogen.

Statistical analysis

Comparison between the average variables of 2 groups was performed by 2-tailed Student's t test. *P*-values less than 0.05 were considered to be statistically significant.

RESULTS

HIF-1α expression is rapidly downregulated at the time point of birth

As a first step in the investigation of the cellular responses in retina against dramatic change in the oxygen environment at the point of birth, we examined the expression patterns of

pVHL, HIF-1α and HIF-2α in the developing retina, details of which have not yet been documented. The expression of pVHL was detected ubiquitously from the inner to the outer side in the retina, and did not change between before and after birth (Fig. 1A–E). In contrast, nuclear staining of HIF-1α was downregulated in the deep retinal layer (neuroblastic layer [NBL] at this stage) after birth (Fig. 1H–J) despite its ubiquitous expression in embryonic stages (Fig. 1F,G). HIF-2α immunoreactivity was predominantly detected in endothelial cells of hyaloid vessels in the vitreal space (Fig. S1A–C) and retinal vessels in the ganglion cell layer (GCL) (Fig. S1D,E). In embryonic retina, hypoxic areas were visualized by hypoxic probe, pimonidazole through all layers (Fig. 1K,L), although a relatively hypoxic area after birth was limited to the GCL (Fig. 1M–O) still expressing HIF-1α (Fig. 1H–J).

VHL$^{\alpha\text{-}Cre\ KO}$ mice show persistence of the hyaloid vessels independently of macrophages

To elucidate the function of pVHL in the postnatal retinal vascularization, we employed a retina-specific Cre line, α-Cre mice, which show Cre-expression in the deep retinal layer including retinal progenitor cell-derived neural cells under control of a neural retina-specific regulatory element of murine *Pax6* gene, but not in astrocytes and endothelial cells at postnatal day 10 (P10) (Marquardt et al., 2001). We examined the past events of Cre expression in α-Cre mice until early postnatal age by crossing α-Cre mice with a reporter transgenic line, CAG-CAT-EGFP mice (Kawamoto et al., 2000). At P6, GFP expression was detected in neural cells in the deep retinal layer, but not in astrocytes and endothelial cells of both retinal and hyaloid vasculature (Fig. S2A–T). Then, we crossed *VHL*$^{floxed/floxed}$ mice (Haase et al., 2001) with α-Cre mice, and generated α-Cre-specific conditional knockout mice for *VHL* (*VHL*$^{\alpha\text{-}Cre\ KO}$ mice). As control littermates for *VHL*$^{\alpha\text{-}Cre\ KO}$ mice, we used *VHL*$^{floxed/floxed}$ mice without α-Cre transgene. At P6, blood flow visualized by intra-cardiac injection of fluorescein isothiocyanate (FITC)-dextran was detected in both hyaloid vessels and retinal vessels of control mice (Fig. 2A,B,E,G,I). In *VHL*$^{\alpha\text{-}Cre\ KO}$ mice, however, there was abundant blood flow in hyaloid vessels, poor flow in retinal vessels, and abundant collateral flow from hyaloid vessels to retinal vessels (Fig. 2C,D,F,H,J). Nonetheless, despite the impaired blood flow, the retinal vascular structure could be detected by immunohistochemistry for platelet-endothelial cell adhesion molecule-1 (PECAM-1) in the *VHL*$^{\alpha\text{-}Cre\ KO}$ mice (Fig. 2F,H). The persistent blood flow in hyaloid vessels in *VHL*$^{\alpha\text{-}Cre\ KO}$ mice prompted us to examine the well known mechanisms of hyaloid vessel regression: reduced perivascular macrophages or Angiopoietin-2 deficiency lead to persistence of the hyaloid vessels (Lobov et al., 2005; Rao et al., 2007). Macrophages around the hyaloid vessels were not significantly changed (Fig. 2K–M), and *colony stimulating factor 1 receptor (csflr)* expression, which correlates with the number of macrophages (Kubota et al., 2009) showed no significant reduction in *VHL*$^{\alpha\text{-}Cre\ KO}$ mice (Fig. 2N). Angiopoietin-2 expression was rather increased in *VHL*$^{\alpha\text{-}Cre\ KO}$ mice (Fig. 2O). Collectively, *VHL*$^{\alpha\text{-}Cre\ KO}$ mice show persistence of the hyaloid vessels independently of macrophages and Angiopoietin-2.

VHL$^{\alpha\text{-}Cre\ KO}$ mice show poorly-formed retinal vessels characterized by excessive vessel regression

As abnormal hyaloid vessel persistence may affect retinal vascularization, we examined details of retinal vessels in *VHL*$^{\alpha\text{-}Cre\ KO}$ mice. In these mice, the entire growth of the retinal vasculature spreading from the optic disc and branching points was significantly reduced compared to control mice ($P = 0.013$ for spreading distance, $P = 0.00012$ for branching points) (Fig. 3A,B,D,E,M,N, Fig. S3A,B). Endothelial tip cells and their filopodia, which are controlled by VEGF and Delta-like 4/Notch pathway (Gerhardt et al., 2003; Hellstrom et al., 2007; Phng et al., 2009), were also significantly reduced in *VHL*$^{\alpha\text{-}Cre\ KO}$ mice ($P = 0\ 0012$ for tip cells; $P = 0.011$ for filopodia) (Fig. 3C,F,0,P). Significant decrease in endothelial proliferation (Fig. 3GJ,Q) and excessive vessel regression (Fig. 3H,K,R) characterized by

empty vascular sleeves (Phng et al., 2009) were also detected in $VHL^{\alpha\text{-}Cre\ KO}$ mice ($P = 7.9\times10^{-5}$ for $BrdU^{+}$ endothelial cells; $P = 0.0044$ for empty sleeves). Empty sleeves were abundantly detected not only in their stalk cell area but also their leading edge, suggesting that vessel regression occurs in both tip cells and stalk cells in $VHL^{\alpha\text{-}Cre\ KO}$ mice. Although it is well known that pVHL regulates the expression of various extracellular matrices (Ohh et al., 1998), Col IV expression was not impaired in $VHL^{\alpha\text{-}Cre\ KO}$ mice. Although the number of pericytes associated with endothelial tubes was not changed in $VHL^{\alpha\text{-}Cre\ KO}$ mice (P =0.395) (Fig. 3I,L,S), detached pericytes were frequently detected just beyond their sprouting edges. Previously, injection of Angiopoietin-2 into the eyes of normal rats was shown to induce a dose-dependent pericyte loss (Hammes et al., 2004), suggesting upregulated Angiopoietin-2 (Fig. 2O) may contribute to pericyte defects in $VHL^{\alpha\text{-}Cre\ KO}$ mice. Collectively, $VHL^{\alpha\text{-}Cre\ KO}$ mice showed poorly-formed retinal vessels presumably due to their persistence of the hyaloid vessels.

Vascular defects in $VHL^{\alpha\text{-}Cre\ KO}$ mice are attributable to ectopic VEGF expression

Intact macrophages and preserved Angiopoietin-2 expression in $VHL^{\alpha\text{-}Cre\ KO}$ mice caused us to expect some other mechanisms which lead to the persistence of the hyaloid vessels. As retinal vascular growth depends on the appropriate spatial distribution of heparin-binding VEGF within the retina (Gerhardt et al., 2003; Kubota et al., 2008; Ruhrberg et al,, 2002; Stalmans et al., 2002), we suspected that the vascular defects in $VHL^{\alpha\text{-}Cre\ KO}$ mice were attributable to their abnormal expression pattern of VEGF. In control mice, VEGF expression was predominantly detected in astrocytes beyond the sprouting edge (Fig. 4A,B,E-H). In $VHL^{\alpha\text{-}Cre\ KO}$ mice, marked expression of VEGF was detected in the deep retinal layer (Fig. 4C,D,I–L), and was coincidental with the area of persistent hyaloid vessels. However, typical VEGF expression in astrocytes beyond the sprouting edge was diminished in $VHL^{\alpha\text{-}Cre\ KO}$ mice despite their astrocyte plexus was normal (Fig. 4M,N). This VEGF expression pattern in $VHL^{\alpha\text{-}Cre\ KO}$ mice is similar to normal VEGF expression in the embryonic retina (Saint-Geniez et al., 2006). By quantitative RT-PCR analysis, more than a 4-fold significant increase ($P = 0.00071$) in *vegfa* expression was detected in the entire retina of $VHL^{\alpha\text{-}Cre\ KO}$ mice (Fig. 4O). Since these expression patterns of VEGF suggested that the vascular defects in $\boldsymbol{VHL}^{\alpha\text{-}Cre\ KO}$ mice could be attributable to ectopic and abundant VEGF expression, we injected a potent VEGF inhibitor, Flt1-Fc chimeric protein (Gerhardt et al., 2003; Kubota et al., 2008), into the eyes of $VHL^{\alpha\text{-}Cre\ KO}$ mice. These Flt1-Fc injections reduced the amounts of both collateral blood flow and vascular structures from hyaloid vessels to retinal vessels (Fig. 4P–U). As genetic inactivation of the VHL gene results in stabilization of HIF-αs (Kapitsinou and Haase, 2008) and upregulation of the expression of *vegfa*, which is widely known as a HIF-1α target gene (Forsythe et al, 1996), we examined the expressions of pVHL, HIF-1α, and HIF-2α in $VHL^{\alpha\text{-}Cre\ KO}$ mice. We found that pVHL immunoreactivity was greatly reduced in the deep layer of the peripheral retina (Fig. 4V,W), where the strong α-Cre-mediated recombination is detected (Fig. S2), except in astrocytes and endothelial cells (Figure S4A–J). HIF-1α–imunoreactivity was increased in this area of $VHL^{\alpha\text{-}Cre\ KO}$ mice (Fig. 4X,Y, Fig. S4K–0). In addition, strong HIF-2α immunoreactivity was detected in invaginating hyaloid vessels, but not in the area of reduced pVHL (Fig. 4Z,AA, Fig. S4P–T).

Increased VEGF expression in $VHL^{\alpha\text{-}Cre\ KO}$ mice is due to their impaired oxygen-sensing mechanism via HIF-1α

As the VEGF expression pattern in postnatal $VHL^{\alpha\text{-}Cre\ KO}$ retina is similar to normal VEGF expression in the embryonic retina (Saint-Geniez et al., 2006), we expected abnormal VEGF expression in $VHL^{\alpha\text{-}Cre\ KO}$ retina is attributable to an impaired oxygen-sensing mechanism and lack of response to atmospheric oxygen concentration. As newborn mice do not tolerate oxygen levels below 10% (Claxton and Fruttiger, 2005), we employed an *ex vivo* retinal

culture system, which enables us to expose the retina to variable oxygen concentration between 1% and 21% (Fig. 5A). In culture of control retina, strong nuclear HIF-1α was induced in 1% oxygen (Fig. 5D), but not in 21% oxygen (Fig. 5B). Consequently, *vegfa* expression was significantly higher ($p = 2.4\times10^{-8}$) in 1% oxygen than in 21% oxygen (Fig. 5J). In culture of *VHL*$^{\alpha\text{-}Cre\ KO}$ retina, strong nuclear HIF-1α was detected (Fig. 5H) even in 21% oxygen (Fig. 5F), and *vegfa* expression in *VHL*$^{\alpha\text{-}Cre\ KO}$ retina in 21% oxygen was significantly higher ($p = 1.1\times10^{-5}$) than in control in 21% oxygen, although it was equivalent to that in 1% oxygen (Fig. 5J). To determine the significance of the increased nuclear HIF-1α level in hypoxic condition in this culture system, we generated α-Cre-mediated conditional knockout mice for HIF-1α (Ryan et al., 2000) (*HIF-1α* $^{\alpha\text{-}Cre\ KO}$ mice). In *HIF-1*$^{\alpha\text{-}Cre\ KO}$ retina, hypoxia-induced HIF-1α stabilization (Fig. 5K.M) was not detected (Fig. 5O,Q), and accordingly, increased *vegfa* expression in 1 % oxygen was significantly suppressed ($p = 0.00028$) compared with control retina (Fig. 5S). Consistent with the *in vivo* results (Fig. 1A–E), the expression pattern of pVHL was stable in the deep retinal layer during *ex vivo* culture, and was not affected by the oxygen concentration (Fig. 5C,E,G,I,L,N,P,R). These data in the *ex vivo* culture system suggest that the increased VEGF expression in *VHL*$^{\alpha\text{-}Cre\ KO}$ mice is due to their impaired oxygen-sensing mechanism via HIF-1 α.

Deletion of HIF-1α, but not HIF-2α, rescues vascular defects in *VHL*$^{\alpha\text{-}Cre\ KO}$ mice

All the expression patterns of pVHL, HIF-1α, HIF-2α, and VEGF in *VHL*$^{\alpha\text{-}Cre\ KO}$ mice (Fig. 4) and the data from the *ex vivo* culture system (Fig. 5) suggested that the increased activity of HIF-1α is responsible for the vascular defects in *VHL*$^{\alpha\text{-}Cre\ KO}$ mice. Therefore, we generated α-Cre-specific double-knockout mice for VHL and HIF-1α (Ryan et al., 2000) (*HIF-1α; VHL*$^{\alpha\text{-}Cre\ KO}$ mice). Vascular defects seen in *VHL*$^{\alpha\text{-}Cre\ KO}$ mice were suppressed in *HIF-1α;VHL*$^{\alpha\text{-}Cre\ KO}$ mice (Fig. 6A,B,D–G,M–P). The abnormal expression of *vegfa* in *VHL*$^{\alpha\text{-}Cre\ KO}$ was fairly normalized in *HIF-lα; VHL*$^{\alpha\text{-}Cre\ KO}$ *mice* (Fig 6J,K; Fig. S5A, 1.15 ± 0.08-fold compared to control). On the other hand, α-Cre-mediated VHL and HIF-2α (Gruber et al., 2007) double-knockout mice (*HIF-2α; VHL*$^{\alpha\text{-}Cre\ KO}$ mice) showed similar vascular defects and VEGF expression pattern to *VHL*$^{\alpha\text{-}Cre\ KO}$ mice (Fig. 6C,H,I,L; Fig. S5B). Taken together, HIF-1α, but not HIF-2α, plays essential roles for the appearance of vascular defects in *VHL*$^{\alpha\text{-}Cre\ KO}$ retina.

Progressive retinal degeneration in adult *VHL*$^{\alpha\text{-}Cre\ KO}$ mice

Next, we examined retinal function and circulation in adult *VHL*$^{\alpha\text{-}Cre\ KO}$ mice. Increased apoptosis of photoreceptors and other neuronal cells was seen in *VHL*$^{\alpha\text{-}Cre\ KO}$ mice after P14 (Fig. 7A–H) induced decrease of ONL (Fig. 7I,J) despite the normal development of photoreceptors at P7 (Fig. 7E,J). Gliosis, accompanied by vessels invaginating into the deep retinal layer, destroyed the construction of ONL (Fig. 7K–T) at P14. As the result, a significant ($P = 3.3\times10^{-6}$ for a-wave, $P = 1.3\times10^{-5}$ for b-wave) decrease in amplitude and a significant ($P = 0.046$ for b-wave) extension of implicit time in electroretinography (ERG) in *VHL*$^{\alpha\text{-}Cre\ KO}$ mice at P28 (Fig. 7U–Y). Circulation via hyaloid vessels in the *VHL*$^{\alpha\text{-}Cre\ KO}$ retina was detected at the age of 8 weeks (Fig. S6A–D) and at 18 months (Fig. S6E–H). Some of the *VHL*$^{\alpha\text{-}Cre\ KO}$ mice developed pre-retinal hemorrhage, cataracts, and iris neovascularization (Fig. 8A–C), similar to phenotypes accompanying ischemic retinopathy (Hayreh, 2007).

DISCUSSION

In the present study, we showed that retina-specific conditional knockout mice for VHL gene exhibit persistent hyaloid vessels independently of macrophage function, which sustain until adult age. These vascular defects in *VHL*$^{\alpha\text{-}Cre\ KO}$ mice are rescued by either local

VEGF inhibition or genetic deletion of HIF-1α, but not HIF-2α. These results suggest not only macrophages but also tissue oxygen-sensing mechanisms regulate the transition from fetal to adult circulatory system in retina.

Considering that HIF-1α in the outer side of the retina is dramatically downregulated after birth while the pVHL expression in the retina does not differ between embryos and neonates (Fig. 1), the change of environmental oxygen concentration must be important for the role of pVHL in this transition (Rodesch et al., 1992). VEGF expression in the deep retinal layer during embryonic retina but not postnatal age (Saint-Geniez et al., 2006) supports the idea that abnormal VEGF distribution in postnatal $VHL^{\alpha\text{-}Cre\ KO}$ retina represents defective VEGF expression switch from embryonic pattern to postnatal one. Mice selectively expressing single isoforms of VEGF ($VEGF_{120}$ or $VEGF_{188}$) or overexpressing VEGF under lens specific promotor show persistence of hyaloid vessels as well as defective retinal vascularization, supporting the concept that spatial distribution of VEGF regulates transition from embryonic to adult circulatory system in retina (Mitchell et al., 2006; Stalmans et al., 2002).

Previously, Lang and colleagues clearly demonstrated that macrophages mediate hyaloid vessel regression by paracrining Wnt7b (Lobov et al., 2005). They showed that a lack of macrophages in $PU.1^{-/-}$ mice caused significant delay in hyaloid vessel regression, and that intra-ocularly injected wild-type but not Wnt7b-mutant macrophages ameliorated this delay. Moreover, Angiopoietin-2 has also been shown to be involved in hyaloid vessel regression via the dual effect of suppressing survival signaling in endothelial cells of hyaloid vessels and stimulating Wnt ligand production by macrophages (Rao et al., 2007). Interestingly, the macrophage/microglia number in $VHL^{\alpha\text{-}Cre\ KO}$ mice was not affected (Fig. 2K–M), and Angiopoietin-2 expression in $VHL^{\alpha\text{-}Cre\ KO}$ mice were rather increased (Fig. 2O), suggesting oxygen-sensing mechanism mediated by the VHL/HIF-1α/VEGF system operate hyaloid vessel regression independently of macrophages, Wnt, and Angiopoietin-2.

One of the major issues in our data may be the slightly, but significantly increased branching points in $HIF\text{-}1\alpha;VHL^{\alpha\text{-}Cre\ KO}$ mice (Fig. 6G,N). Independently of HIF-α proteolysis, pVHL is known to be involved in extracellular matrix assembly and turnover (Ohh et al., 1998). Moreover, erythropoietin has been reported to be regulated by VHL and HIFs (Chen et al., 2008; Rankin et al., 2007). These previous findings suggest the involvement of multiple candidates in addition to HIF-1α and VEGF, and may explain the minor vascular changes in $HIF\text{-}1\alpha;VHL^{\alpha\text{-}Cre\ KO}$ mice. However, dramatic rescue effects obtained by Fltl-Fc injection (Fig. 4P–U) or gene inactivation of HIF-1α, but not HIF-2α (Fig. 6) show that the VHL/HIF-1α/VEGF cascade plays crucial roles in the transition from fetal to adult circulatory system in the retina.

Our current study involves various aspects of possible clinical implications. Adult $VHL^{\alpha\text{-}Cre\ KO}$ mice show similar characteristics (Fig. 8) to human ischemic retinopathies such as diabetic retinopathy, retinal vessel occlusion, and retinopathy of prematurity (Hayreh, 2007), providing a clue for exploring mechanisms of these human diseases. It has been recently shown that systemic administration of a PHD inhibitor protects from retinal vaso-obliteration in response to hyperoxia (Sears et al., 2008), suggesting pVHL also functions in retinopathy of prematurity.

Retinal hemangioma in VHL patients and ischemic retinopathies are usually treated by laser photocoagulation that disrupts photoreceptors and increases the oxygen supply for the other neural cells from the choroidal vasculature bed although it may cause night blindness and visual field defects (Yu and Cringle, 2001). Recently, various kinds of VEGF inhibitors (Brown and Regillo, 2007) have become possible candidates for use against ophthalmic

diseases, although destruction of the physiological vasculature (Fischer et al., 2007) and neuronal dysfunction (Saint-Geniez et al., 2008) caused by long-term VEGF inhibition raise caution about the continuous administration of these reagents. Suppression of HIF-1α may be one of the alternative strategies against these diseases in the future.

Finally, all of the results presented suggest that oxygen-sensing mechanisms mediated by VHL/HIF-1α/VEGF regulate the transition from fetal to adult circulatory system in retina, and may represent a theoretical basis for the retinal vascular abnormalities in human VHL disease and the development of ischemic retinopathies. It will be interesting to determine whether this oxygen sensing system, the VHL/HIF-1α pathway, is involved in the transition of the circulatory system in other parts such as ductus arteriosus, which would confirm its generality for future studies.

Supplementary Material

Refer to Web version on PubMed Central for supplementary material.

Acknowledgments

We thank Ichie Kawamori, Rie Takeshita, Haruna Koizumi, and Taiga Shioda (Keio University, Tokyo, Japan) for technical assistance.

This study was supported by the Japanese Ministry of Education, Culture, Sports, Science and Technology (MEXT) (Grant-in-Aid for the 21 st Century COE Program and Global COE Program at Keio University, and Scientific Research [No. 21791710] to T.K.). Y.K. was supperted by Keio Kanrinmaru Project. Experiments using the anti-HIF-la antibody were supported by Japan Society for the Promotion of Science Grant-in-Aid for Creative Scientific Research 17GS0419. M.S. is the Leader of the Global COE Program for Human Metabolomic Systems Biology and H.O. is the Leader of the Global COE Program for Stem Cell Medicine supported by MEXT.

References

Brown DM, Regillo CD. Anti-VEGF agents in the treatment of neovascular age-related macular degeneration: applying clinical trial results to the treatment of everyday patients. Am J Ophthalmol. 2007; 144:627–37. [PubMed: 17893015]

Chen J, Connor KM, Aderman CM, Smith LE. Erythropoietin deficiency decreases vascular stability in mice. J Clin Invest. 2008; 118:526–33. [PubMed: 18219389]

Claxton S, Fruttiger M. Oxygen modifies artery differentiation and network morphogenesis in the retinal vasculature. Dev Dyn. 2005; 233:822–8. [PubMed: 15895398]

Fischer C, Jonckx B, Mazzone M, Zacchigna S, Loges S, Pattarini L, Chorianopoulos E, Liesenborghs L, Koch M, De Mol M, et al. Anti-PIGF inhibits growth of VEGF(R)-inhibitor-resistant tumors without affecting healthy vessels. Cell. 2007; 131:463–75. [PubMed: 17981115]

Forsythe JA, Jiang BH, Iyer NV, Agani F, Leung SW, Koos RD, Semenza GL. Activation of vascular endothelial growth factor gene transcription by hypoxia-inducible factor 1. Mol Cell Biol. 1996; 16:4604–13. [PubMed: 8756616]

Fruttiger M, Calver AR, Kruger WH, Mudhar HS, Michalovich D, Takakura N, Nishikawa S, Richardson WD. PDGF mediates a neuron-astrocyte interaction in the developing retina. Neuron. 1996; 17:1117–31. [PubMed: 8982160]

Gerhardt H, Golding M, Fruttiger M, Ruhrberg C, Lundkvist A, Abramsson A, Jeltsch M, Mitchell C, Alitalo K, Shima D, et al. VEGF guides angiogenic sprouting utilizing endothelial tip cell filopodia. J Cell Biol. 2003; 161:1163–77. [PubMed: 12810700]

Gnarra JR, Ward JM, Porter FD, Wagner JR, Devor DE, Grinberg A, Emmert-Buck MR, Westphal H, Klausner RD, Linehan WM. Defective placental vasculogenesis causes embryonic lethality in VHL-deficient mice. Proc Natl Acad Sci USA. 1997; 94:9102–7. [PubMed: 9256442]

Gruber M, Hu CJ, Johnson RS, Brown EJ, Keith B, Simon MC. Acute postnatal ablation of Hif-2alpha results in anemia. Proc Natl Acad Sci USA. 2007; 104:2301–6. [PubMed: 17284606]

Haase VH, Glickman JN, Socolovsky M, Jaenisch R. Vascular tumors in livers with targeted inactivation of the von Hippel-Lindau tumor suppressor. Proc Natl Acad Sci USA. 2001; 98:1583–8. [PubMed: 11171994]

Hammes HP, Lin J, Wagner P, Feng Y, Vom Hagen F, Krzizok T, Renner O, Breier G, Brownlee M, Deutsch U. Angiopoietin-2 causes pericyte dropout in the normal retina: evidence for involvement in diabetic retinopathy. Diabetes. 2004; 53:1104–10. [PubMed: 15047628]

Hayreh SS. Neovascular glaucoma. Prog Retin Eye Res. 2007; 26:470–85. [PubMed: 17690002]

Hellstrom M, Phng LK, Hofmann JJ, Wallgard E, Coultas L, Lindblom P, Alva J, Nilsson AK, Karlsson L, Gaiano N, et al. Dll4 signalling through Notch 1 regulates formation of tip cells during angiogenesis. Nature. 2007; 445:776–80. [PubMed: 17259973]

Hu CJ, Wang LY, Chodosh LA, Keith B, Simon MC. Differential roles of hypoxia-inducible factor 1 alpha (HIF-1 alpha) and HIF-2alpha in hypoxic gene regulation. Mol Cell Biol. 2003; 23:9361–74. [PubMed: 14645546]

Kapitsinou PP, Haase VH. The VHL tumor suppressor and HIF: insights from genetic studies in mice. Cell Death Differ. 2008; 15:650–9. [PubMed: 18219317]

Kawamoto S, Niwa H, Tashiro F, Sano S, Kondoh G, Takeda J, Tabayashi K, Miyazaki J. A novel reporter mouse strain that expresses enhanced green fluorescent protein upon Cre-mediated recombination. FEBS Lett. 2000; 470:263–8. [PubMed: 10745079]

Kubota Y, Hiroshima M, Kishi K, Stewart CL, Suda T. Leukemia inhibitory factor regulates microvessel density by modulating oxygen-dependent VEGF expression in mice. J Clin Invest. 2008; 118:2393–403. [PubMed: 18521186]

Kubota Y, Takubo K, Shimizu T, Ohno H, Kishi K, Shibuya M, Saya H, Suda T. M-CSF inhibition selectively targets pathological angiogenesis and lymphangiogenesis. J Exp Med. 2009; 206:1089–102. [PubMed: 19398755]

Kurihara T, Ozawa Y, Shinoda K, Nagai N, Inoue M, Oike Y, Tsubota K, Ishida S, Okano H. Neuroprotective effects of angiotensin II type 1 receptor (AT1R) blocker, telmisartan, via modulating AT1R and AT2R signaling in retinal inflammation. Invest Ophthalmol Vis Sci. 2006; 47:5545–52. [PubMed: 17122147]

Lang RA. Apoptosis in mammalian eye development: lens morphogenesis, vascular regression and immune privilege. Cell Death Differ. 1997; 4:12–20. [PubMed: 16465205]

Lang RA, Bishop JM. Macrophages are required for cell death and tissue remodeling in the developing mouse eye. Cell. 1993; 74:453–62. [PubMed: 8348612]

Lobov IB, Rao S, Carroll TJ, Vallance JE, Ito M, Ondr JK, Kurup S, Glass DA, Patel MS, Shu W, et al. WNT7b mediates macrophage-induced programmed cell death in patterning of the vasculature. Nature. 2005; 437:417–21. [PubMed: 16163358]

Marquardt T, Ashery-Padan R, Andrejewski N, Scardigli R, Guillemot F, Gruss P. Pax6 is required for the multipotent state of retinal progenitor cells. Cell. 2001; 105:43–55. [PubMed: 11301001]

Maxwell PH, Wiesener MS, Chang GW, Clifford SC, Vaux EC, Cockman ME, Wykoff CC, Pugh CW, Maher ER, Ratcliffe PJ. The tumour suppressor protein VHL targets hypoxia-inducible factors for oxygen-dependent proteolysis. Nature. 1999; 399:271–5. [PubMed: 10353251]

Merkle EM, Gilkeson RC. Remnants of fetal circulation: appearance on MDCT in adults. AJR Am J Roentgenol. 2005; 185:541–9. [PubMed: 16037534]

Mitchell CA, Rutland CS, Walker M, Nasir M, Foss AJ, Stewart C, Gerhardt H, Konerding MA, Risau W, Drexler HC. Unique vascular phenotypes following over-expression of individual VEGFA isoforms from the developing lens. Angiogenesis. 2006; 9:209–24. [PubMed: 17109192]

Nicholson DH, Green WR, Kenyon KR. Light and electron microscopic study of early lesions in angiomatosis retinae. Am J Ophthalmol. 1976; 82:193–204. [PubMed: 986118]

Ohh M, Yauch RL, Lonergan KM, Whaley JM, Stenuner-Rachamimov AO, Louis DN, Gavin BJ, Kley N, Kaelin WG Jr, Iliopoulos O. The von Hippel-Lindau tumor suppressor protein is required for proper assembly of an extracellular fibronectin matrix. Mol Cell. 1998; 1:959–68. [PubMed: 9651579]

Ozawa Y, Nakao K, Shimazaki T, Shimmura S, Kurihara T, Ishida S, Yoshimura A, Tsubota K, Okano H. SOCS3 is required to temporally fine-tune photoreceptor cell differentiation. Dev Biol. 2007; 303:591–600. [PubMed: 17198696]

Ozawa Y, Nakao K, Shimazaki T, Takeda J, Akira S, Ishihara K, Hirano T, Oguchi Y, Okano H. Downregulation of STAT3 activation is required for presumptive rod photoreceptor cells to differentiate in the postnatal retina. Mol Cell Neurosci. 2004; 26:258–70. [PubMed: 15207851]

Phng LK, Potente M, Leslie JD, Babbage J, Nyqvist D, Lobov L, Ondr JK, Rao S, Lang RA, Thurston G, et al. Nrarp coordinates endothelial Notch and Wnt signaling to control vessel density in angiogenesis. Dev Cell. 2009; 16:70–82. [PubMed: 19154719]

Rankin EB, Biju MP, Liu Q, Unger TL, Rha J, Johnson RS, Simon MC, Keith B, Haase VH. Hypoxia-inducible factor-2 (HIF-2) regulates hepatic erythropoietin in vivo. J Clin Invest. 2007; 117:1068–77. [PubMed: 17404621]

Rao S, Lobov IB, Vallance JE, Tsujikawa K, Shiojima I, Akunuru S, Walsh K, Benjamin LE, Lang RA. Obligatory participation of macrophages in an angiopoietin 2-mediated cell death switch. Development. 2007; 134:4449–58. [PubMed: 18039971]

Rodesch F, Simon P, Donner C, Jauniaux E. Oxygen measurements in endometrial and trophoblastic tissues during early pregnancy. Obstet Gynecol. 1992; 80:283–5. [PubMed: 1635745]

Ruhrberg C, Gerhardt H, Golding M, Watson R, Ioannidou S, Fujisawa H, Betsholtz C, Shima DT. Spatially restricted patterning cues provided by heparin-binding VEGF-A control blood vessel branching morphogenesis. Genes Dev. 2002; 16:2684–98. [PubMed: 12381667]

Ryan HE, Poloni M, McNulty W, Elson D, Gassmann M, Arbeit JM, Johnson RS. Hypoxia-inducible factor-1 alpha is a positive factor in solid tumor growth. Cancer Res. 2000; 60:4010–5. [PubMed: 10945599]

Saint-Geniez M, Maharaj AS, Walshe TE, Tucker BA, Sekiyama E, Kurihara T, Darland DC, Young MJ, D'Amore PA. Endogenous VEGF is required for visual function: evidence for a survival role on muller cells and photoreceptors. PLoS ONE. 2008; 3:e3554. [PubMed: 18978936]

Saint-Geniez M, Maldonado AE, D'Amore PA. VEGF expression and receptor activation in the choroid during development and in the adult. Invest Ophthalmol Vis Sci. 2006; 47:3135–42. [PubMed: 16799060]

Sears JE, Hoppe G, Ebrahem Q, Anand-Apte B. Prolyl hydroxylase inhibition during hyperoxia prevents oxygen-induced retinopathy. Proc Natl Acad Sci U S A. 2008; 105:19898–903. [PubMed: 19057008]

Stalmans I, Ng YS, Rohan R, Fruttiger M, Bouche A, Yuce A, Fujisawa H, Hermans B, Shard M, Jansen S, et al. Arteriolar and venular patterning in retinas of mice selectively expressing VEGF isoforms. J Clin Invest. 2002; 109:327–36. [PubMed: 11827992]

Tang N, Mack F, Haase VH, Simon MC, Johnson RS. pVHL function is essential for endothelial extracellular matrix deposition. Mol Cell Biol. 2006; 26:2519–30. [PubMed: 16537898]

Yu DY, Cringle SJ. Oxygen distribution and consumption within the retina in vascularised and avascular retinas and in animal models of retinal disease. Prog Retin Eye Res. 2001; 20:175–208. [PubMed: 11173251]

Yun Z, Maecker HL, Johnson RS, Giaccia AJ. Inhibition of PPAR gamma 2 gene expression by the HIF-1-regulated gene DEC1/Stral3: a mechanism for regulation of adipogenesis by hypoxia. Dev Cell. 2002; 2:331–41. [PubMed: 11879638]

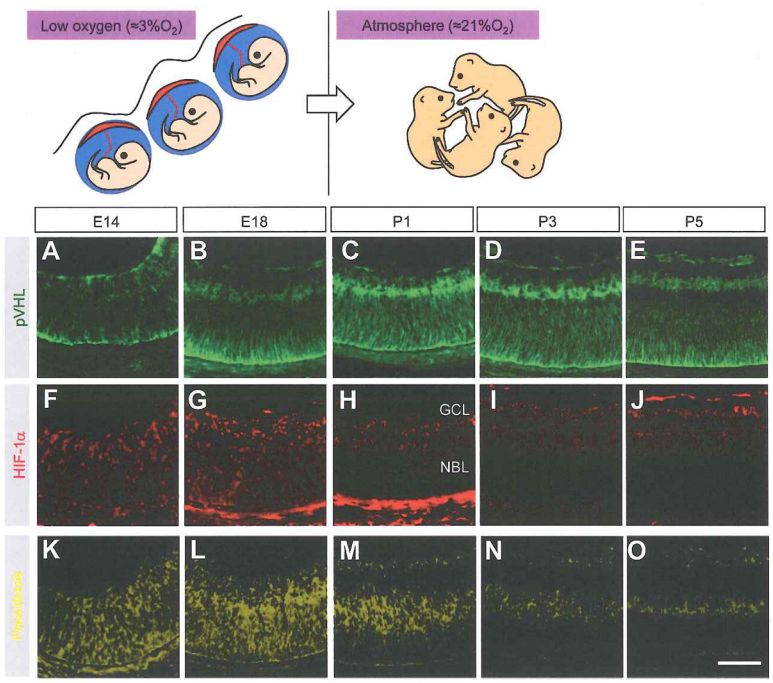

Fig. 1. Expression patterns of pVHL and HIF-1α in the retina before and after birth

(A–E) pVHL staining (green), detected in the soma of cells in the whole retina, is not changed between before and after birth. (F–J) Nuclear staining of HIF-1α (red), detected ubiquitously in embryo (F,G), is downregulated in the deep retinal layer (NBL at this stage) after birth (H–J). (K–O) In embryonic retina, hypoxic areas visualized by hypoxic probe, pimonidazole (yellow), spread all through the layers (K,L), although after birth, hypoxic signal was considerably downregulated in the retina, noticeably in the deep retinal layer (M–O) where HIF-1α expression has also declined (H–J). Scale bars: 100 μm in (A–O). GCL, ganglion cell layer; NBL, neuroblastic layer

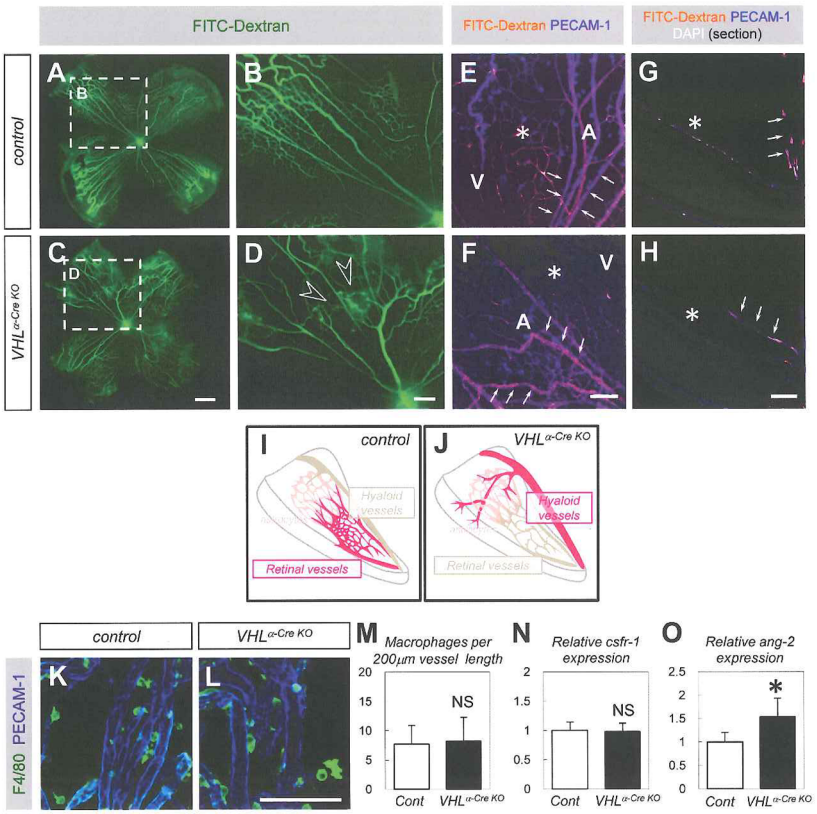

Fig. 2. *VHL*$^{\alpha\text{-}Cre\ KO}$ mice show persistence of the hyaloid vessels independently of macrophages

(A–D) Representative images for the retinas after intra-cardiac FITC injection (n=8). *VHL*$^{\alpha\text{-}Cre\ KO}$ mice show collateral flow from hyaloid vessels to retinal vessels (open arrowheads) in the P6 retinas. Blood flow was visualized by intra-cardiac FITC-conjugated dextran (green) injections. (E–H) Confocal images of FITC (orange) labeled with PECAM-1 (blue) in P6 retinas. Panels G,H show images for the section specimens. Poor blood flow is detected in retinal vasculature (asterisk) in *VHL*$^{\alpha\text{-}Cre\ KO}$ mice compared to control. Relatively abundant dextran was perfused into arteries (A), veins (V) in control mice, and into hyaloid vessels (arrows) in *VHL*$^{\alpha\text{-}Cre\ KO}$ mice. (I,J) Schematics show abundant blood flow (red) in retinal vessels in control mice, and in hyaloid vessels in *VHL*$^{\alpha\text{-}Cre\ KO}$ mice. (K,L) Immunostaining with F4/80 (green) and PECAM-1 (blue) on hyaloid vessels in P6 retinas. (M) Quantification of F4/80^{+} macrophages per 200μm vessel length. Vessel length was calculated by FV10-ASW Viewer software (n = 4). (N,0) Quantitative PCR of *csflr* (N) *or angiopoietin-2* (O) for isolated RNA from P6 retinas (n = 5). Scale bars: 500 μm in (A–D); 100 μm in (E-H,K,L). *P < 0.05. All panels are on P6 retina. All error bars indicate mean ± s.d.

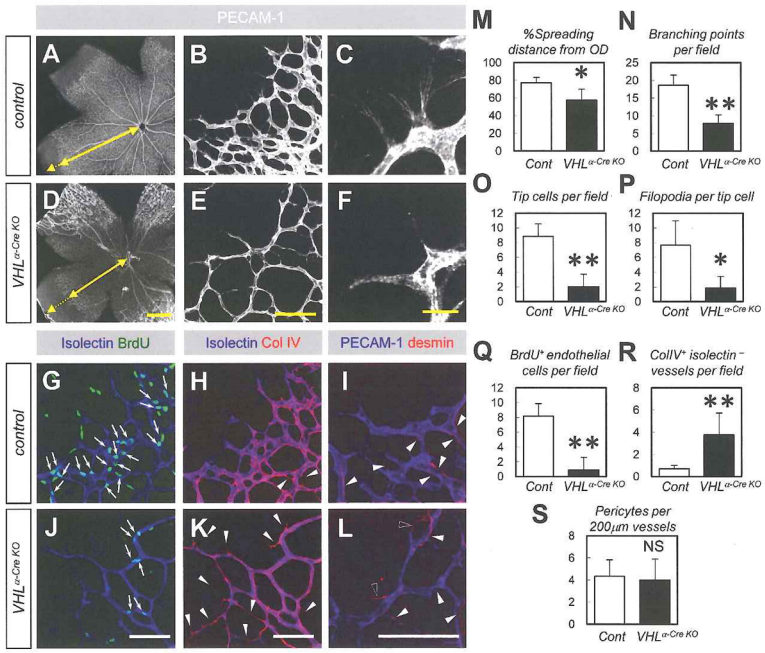

Fig. 3. *VHL*$^{\alpha\text{-}Cre\ KO}$ mice show poorly-formed retinal vessels characterized by excessive vessel regression

(A–F) PEC AM-1 staining of P6 retinas. Note delayed vascular growth (bidirectional arrows in [A,D]), decreased branching points and tip cells (B,E), and filopodia (C,F) in *VHL*$^{\alpha\text{-}Cre\ KO}$ mice. Persistent hyaloid vessels in the lower left lobe of *VHL*$^{\alpha\text{-}Cre\ KO}$ mice were removed mechanically before immunostaining (D). (G–L) Immunostaining with indicated antibodies. Note the decreased BrdU^{+} endothelial cells (arrows in [G,J]), type IV collagen (Col IV)$^{+}$isolectin^{-} empty sleeves (arrowheads in [H,K]), and detached pericytes beyond sprouting edges (open arrowheads in [L]) in *VHL*$^{\alpha\text{-}Cre\ KO}$ mice although most pericytes in control mice are closely contacted with vasculature (closed arrowheads in [I,L]). (M–S) Quantification of %spreading distance from optic discs (M), number of branching points in the area behind sprouting edges (N), tip cells per field (O), filopodia per tip cell (P), BrdU^{+} endothelial cells (Q), Col IV^{+}isolectin^{-} vessels (R), and pericytes per 200 μm vessel length (S) (n = 6, in each genotype). Scale bars: 500 μm in (A,D); 100 μm in (B,E,G–L). 20 μm in (C,F). *P < 0.05, **P < 0.01. All panels are on P6 retina. All error bars indicate mean ± s.d.

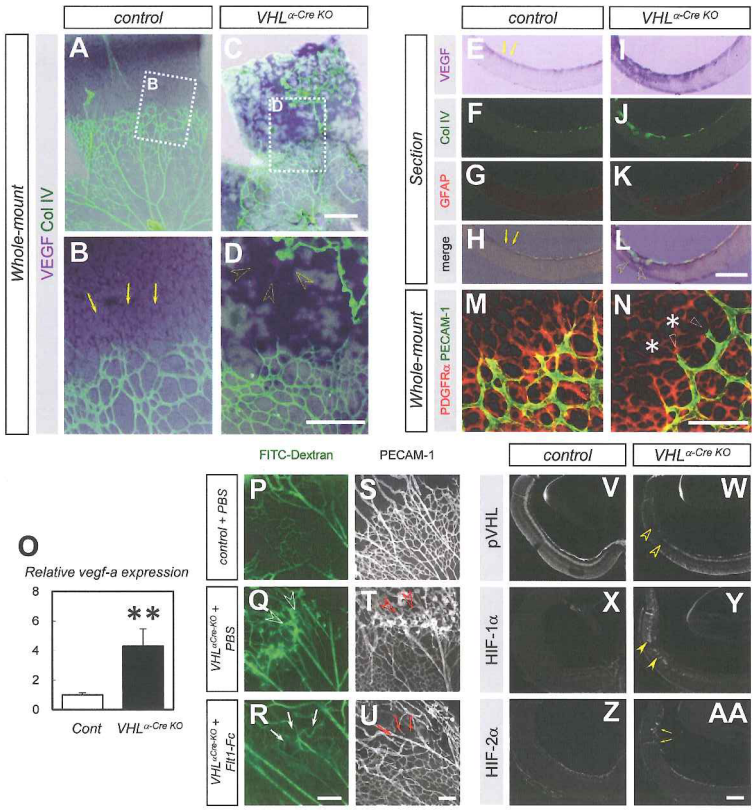

Fig. 4. Vascular defects in *VHL*$^{\alpha\text{-}Cre\ KO}$ mice are attributable to ectopic VEGF expression

(A–L) Whole-mount (A–D) or section (E–L) *in situ* hybridization for VEGF combined with immunostaining with indicated antibodies. Although VEGF expression is detected in astrocytes located in avascular area (arrows) of control mice, abundant VEGF expression is detected in the deep retinal layer (open arrowheads) where persistent hyaloid vessels invaginate in *VHL*$^{\alpha\text{-}Cre\ KO}$ mice. (M,N) Immunostaining with PEC AM-1 (green) and PDGFRα (red) on P6 retinas. Despite normal astrocyte plexus (asterisks), vessel regression (open arrowheads) occurs in *VHL*$^{\alpha\text{-}Cre\ KO}$ mice. (O) Quantitative PCR of *vegfa* for isolated RNA from P6 retinas ($n = 6$). (P–U) Fluorescent microscopic images in P6 retinas perfused with FITC-dextran (P–R), and confocal images labeled with PECAM-1 (S–U). Flt1-Fc injection into the eyes of *VHL*$^{\alpha\text{-}Cre\ KO}$ mice reduces collateral flow (arrows in Q) and vascular structures (arrows in U) that exist abundantly in *VHL*$^{\alpha\text{-}Cre\ KO}$ mice injected with vehicle (open arrowheads in Q,T). (V-AA) Immunostaining with indicated antibodies for sections of P6 retinas. While pVHL-expression is greatly reduced (open arrowheads in W), HIF-1α-immunoreactivity is increased (closed arrowheads in Y) in the deep retinal layer of *VHL*$^{\alpha\text{-}Cre\ KO}$ mice. HIF-2α staining is detected in invaginating hyaloid vessels in *VHL*$^{\alpha\text{-}Cre\ KO}$ (arrows in AA) Scale bars: 500 μm in (A–L). 200 μm in (P-AA); 100 μm in (M,N). $^{**}P < 0.01$. All error bars indicate mean ± s.d.

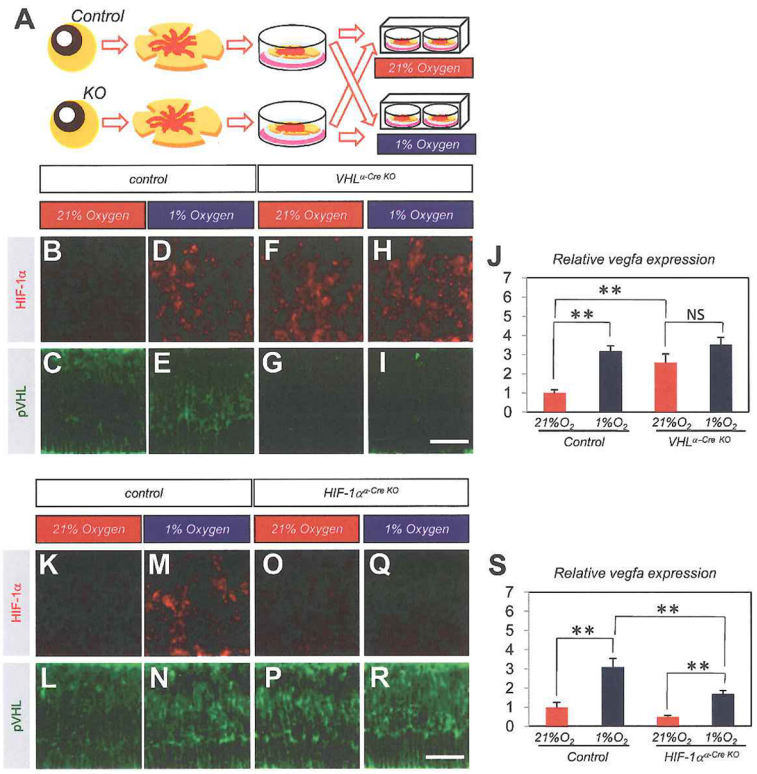

Fig. 5. Increased VEGF expression in *VHL*$^{\alpha\text{-}Cre\ KO}$ mice is due to their impaired oxygen-sensing mechanism via HIF-1α

(A) Schematics show the experimental procedure, illustrating that isolated retinas from control or conditional knockout mice were unfolded, placed on a chamber filter, and exposed to each concentration of oxygen. Retinal explants of control mice (B–E,K–N), *VHL*$^{\alpha\text{-}Cre\ KO}$ mice (F–I), or *HIF-1α* $^{\alpha\text{-}Cre\ KO}$ mice (O–R) were exposed to 21% oxygen (B,C,F,G,K,L,O,P) or 1% oxygen (D,E,H,I,M,N,Q,R). (J,S) Quantitative PCR of *vegfa* for isolated RNA from retinal explants (n = 6, respectively). Note strong HIF-loc staining (red) is induced by 1% oxygen (D,H,M) except in *HIF-1α* $^{\alpha\text{-}Cre\ KO}$ retina (Q), or gene inactivation of VHL (F,H). The expression of pVHL was not detected in *VHL*$^{\alpha\text{-}Cre\ KO}$ retina (G,I). Correlated with the expression of HIF-1α, *vegfa* expression was upregulated even in normoxia status in *VHL*$^{\alpha\text{-}Cre\ KO}$ retina (J). In *HIF-1α* $^{\alpha\text{-}Cre\ KO}$ retina, hypoxia-induced *vegfa* expression was significantly suppressed (S). Scale bars: 50 μ in (B–I,K–R.). $^{**}p < 0.01$. All error bars indicate mean ± s.d.

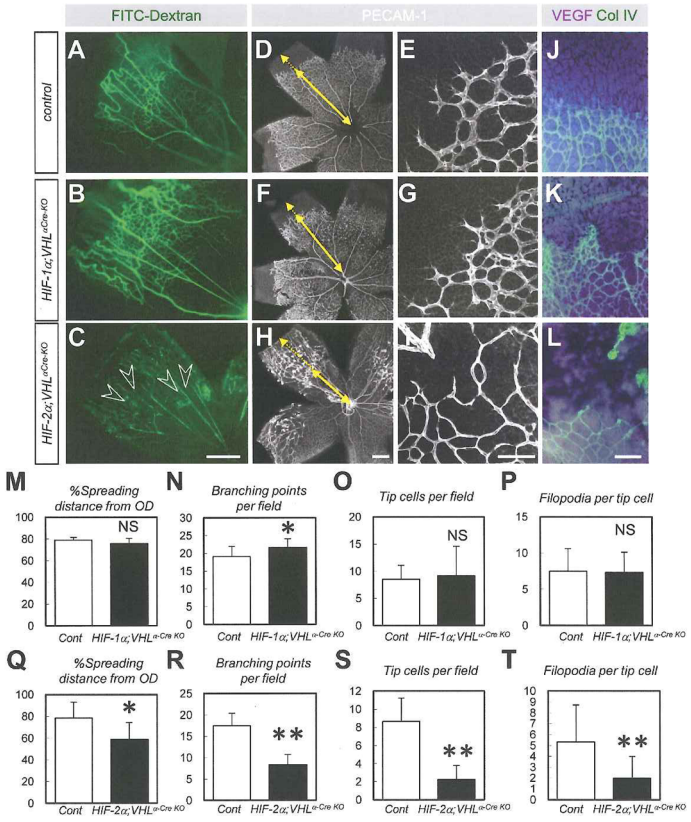

Fig. 6. Deletion of HIF-1α but not HIF-2α rescues vascular defects in *VHL*$^{\alpha\text{-}Cre\ KO}$ mice

(A–L) Blood flow visualized by intra-cardiac FITC-dextran injection (A–C), or confocal images labeled with PECAM-1 at P6 (D–I). Vascular defects (collateral flow from hyaloid vessels to retinal vessels [open arrowheads], delayed vascular growth [bidirectional arrows], decreased branching points, tip cells and filopodia) seen in *VHL*$^{\alpha\text{-}Cre\ KO}$ mice are abolished by deletion of HIF-1α but not HIF-2α in *VHL*$^{\alpha\text{-}Cre\ KO}$ mice. Whole-mount *in situ* hybridization for VEGF combined with immunostaining with Col IV (green). Ectopic VEGF expression seen in *VHL*$^{\alpha\text{-}Cre\ KO}$ mice are abolished by deletion of HIF-1 α but not HIF-2α in *VHL*$^{\alpha\text{-}Cre\ KO}$ mice (J–L). (M–T) Quantification of %spreading distance from optic discs (M,Q), number of branching points in the area behind sprouting edges (N,R), tip cells per field (O,S), filopodia per tip cell (P,T) (n = 6, in each genotype). Scale bars: 500 μm in (A–C,D,F,H); 100 μm in (E,G,I,J–L). *P < 0.05, **P < 0.01. All error bars indicate mean ± s.d.

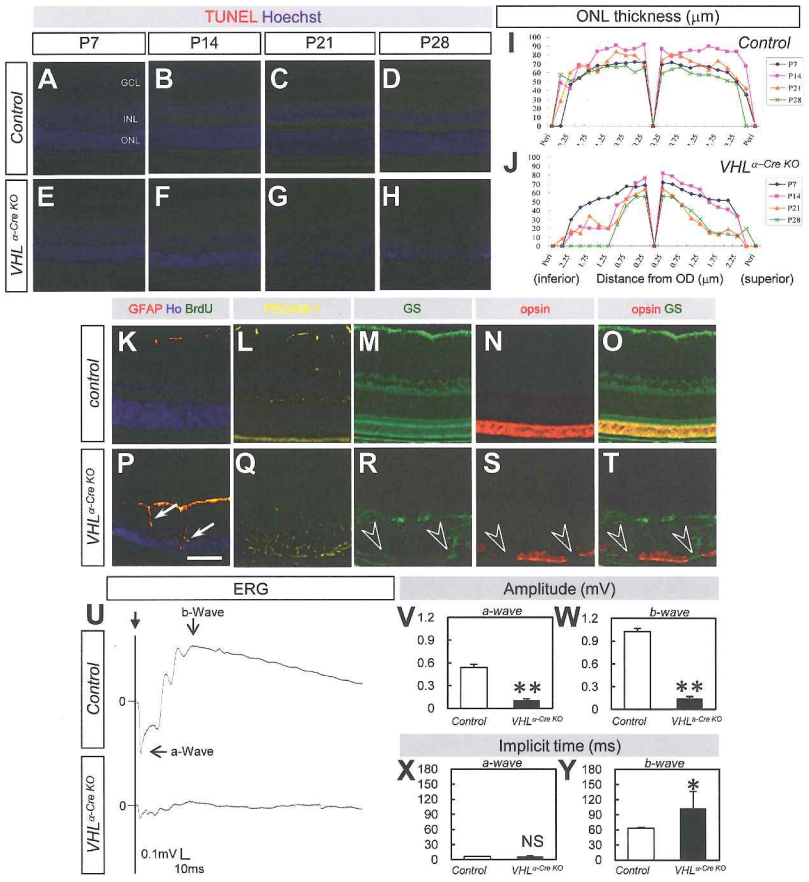

Fig. 7. *VHL*$^{\alpha\text{-}Cre\ KO}$ mice develop retinal degeneration in adult

(A–H) TUNEL-positive cells (red) in counterstaining with Hoechst (blue) are increased in ONL in *VHL*$^{\alpha\text{-}Cre\ KO}$ mice (E–H) compared to control mice (A–D) after P14. (I,J) ONL thickness is decreased time-dependently in *VHL*$^{\alpha\text{-}Cre\ KO}$ mice (n = 3, respectively). (K–T) Merged image for glial fibrillary acidic protein (GFAP), Hoechst, and BrdU (K,P), and IHC for PECAM-1 (yellow in [L,Q]), glutamine synthetase (GS, green in [M,R]), opsin (red in [N,S]), and merged image for GS and opsin (O,T) in control (K–O) or *VHL*$^{\alpha\text{-}Cre\ KO}$ mice (P–T). Proliferating reactive glia is detected by BrdU (arrows in [P]), and gliosis destroys the construction of ONL (open arrowheads in [R–T]) in *VHL*$^{\alpha\text{-}Cre\ KO}$ mice at P14. (U–Y) ERG analysis at P28. Representative wave responses from an individual mouse in control or *VHL*$^{\alpha\text{-}Cre\ KO}$ mice (U). Decreased amplitude (V,W) and prolonged implicit time (Y) are detected in *VHL*$^{\alpha\text{-}Cre\ KO}$ mice (n = 6). Scale bars: 100 μm in (A–H, K–T). GCL, ganglion cell layer; INL, inter nuclear layer; ONL, outer nuclear layer. *P < 0.05, **P < 0.01. All error bars indicate mean ± s.d.

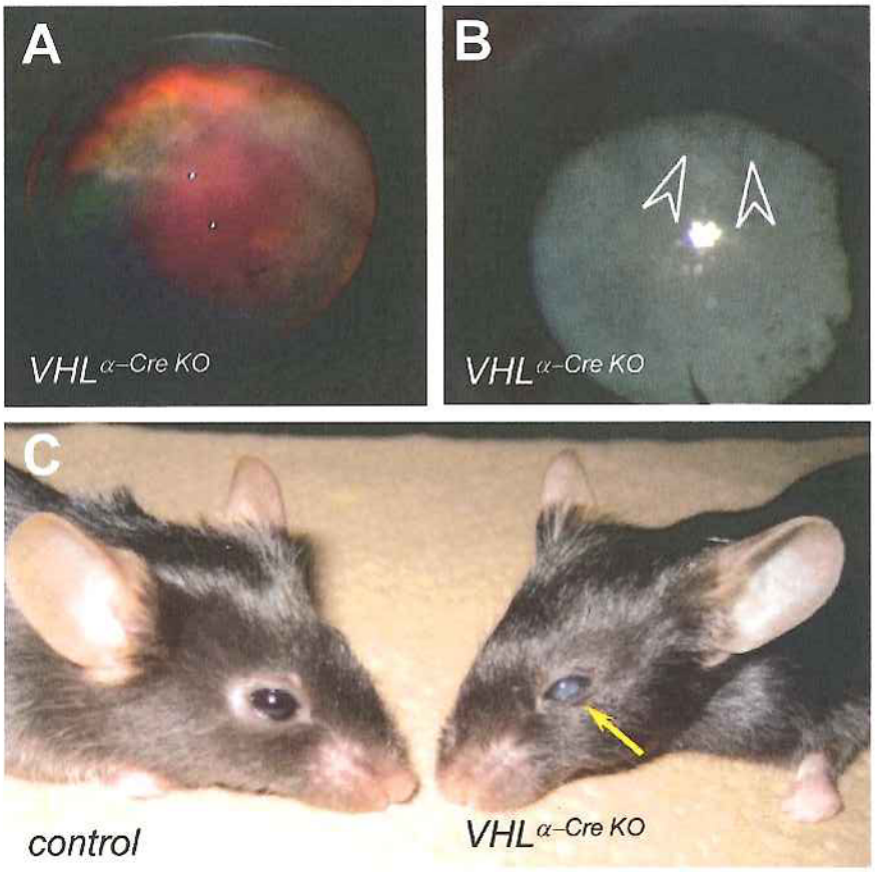

Fig. 8. *VHL*$^{\alpha\text{-}CreKO}$ mice show phenotypes of hypoxic retinopathies

(A) pre-retinal hemorrhage observed by fundus photography, (B) iris neovascularization (open arrowheads), and (C) cataract formation (arrow) in *VHL*$^{\alpha\text{-}Cre\ KO}$ mice.